

HYDRAULIC PERFORMANCE OF A NEW ISOKINETIC TURBINE FOR RIVERS AND ARTIFICIAL CHANNELS

VLAD HASMATUCHI⁽¹⁾, SEBASTIEN ALLIGNE⁽²⁾, JEAN-LOUIS KUENY⁽²⁾ & CECILE MUNCH⁽¹⁾

⁽¹⁾ *University of Applied Sciences and Arts Western Switzerland, Engineering School, Sion, Switzerland,
vlad.hasmatuchi@hevs.ch, cecile.muench@hevs.ch*

⁽²⁾ *Optydro Concept Sàrl, Sion, Switzerland,
sebastien.alligne@powervision-eng.ch, jl.kueny@optydro.ch*

ABSTRACT

A new ducted isokinetic turbine for rivers and artificial channels has been designed. The new (patented) concept consists on an axial turbine with two joined concentric runners: an annular turbine runner and a central pump runner. The aim of the pump runner is to induce a suction effect in the central area in order to increase the axial velocity passing through the turbine runner and consequently the hydraulic efficiency.

In a first step, steady incompressible monophasic turbulent flow (k- ϵ model) numerical simulations have been used to optimize the hydraulic profile of a turbine with an expected mechanical power of 1 kW. A reduced computational domain including only a periodic quart of the turbine (at prototype scale) immersed in a water box has been considered. The Fine/Turbo package of the Numeca commercial code has been employed to solve the RANS equations using the finite volume method. Then, numerical simulations of unsteady incompressible homogeneous multiphase turbulent flow (using the SST model) have been performed on a computational domain including the full water passage of the final prototype, placed in a in a run-of-river tailrace canal with trapezoidal cross-section, to recover its hydraulic efficiency. The URANS equations have been solved with the Ansys CFX 14.5.7 commercial code using the finite volume method.

The main contribution of this work consists on a successful implementation of the numerical tools to optimize and to recover the hydraulic efficiency of a new isokinetic turbine with and without the free-surface effects taken into account. Moreover, the effect of the pump runner is assessed by comparing the obtained efficiency with performances of the isokinetic turbine featuring a free central open passage.

Keywords: isokinetic turbine prototype, hydraulic performance, numerical simulation, free-surface

1. INTRODUCTION

An alternative way to recover the energy of flowing water, other than conventional hydroelectric facilities based on dams and penstocks, is offered by an emerging class of renewable energy technology: the hydrokinetic conversion device (Lago et al., 2010). Indeed, the latest may be deployed both in natural streams (rivers, tidal estuaries, ocean currents) and in artificial waterways (e.g. canals). The most part of isokinetic turbine concepts are inspired from wind technology. Nevertheless, the hydrokinetic technology of turbines may be divided in two main classes: horizontal and vertical systems (Khan et al. 2009). In-between these two, there are the so-called cross-flow systems or Venturi as well as the ones considered as non-turbine (flutter vane, piezoelectric, oscillating hydrofoils, etc.). Moreover, horizontal turbines may present a strait or an inclined axis, coupled with a generator outside the water or immersed. Finally, the mounting of the isokinetic turbine can be done on a floating structure or on a fix one, either on the bottom or on the bank.

Despite its many advantages over conventional hydropower, the hydrokinetic technology has lower power densities, which often makes it hardly economically feasible (Gaden and Bibeau, 2010). Actually, the hydraulic performance of isokinetic turbines placed in free-stream cannot exceed the theoretical limit of Betz (Guney 2011): a power coefficient maximum equal with about 0.59. But in reality, for standard wind turbines, this coefficient does not pass even 0.42 (Heier 1998). On the other hand, it was largely demonstrated, both theoretically and/or in practice (e.g. Igra 1981), that placing the runner in a duct allows going over this limit and implicitly increasing the output power. Moreover, it provides improved safety, protection from weed growth, and of course it allows reducing the turbine and the gear box size for a given power output (Kirke 2006).

The hydrokinetic technology is still relatively young, being concentrated mostly on the recovery of energy from ocean currents. The proof is the presence of a relatively numerous recent studies in the literature focused on the development of new isokinetic turbines (Belloni 2013; O'Doherty et al. 2009; Luquet et al. 2013; Münch et al. 2009), going from design and optimization to numerical flow investigation and to hydraulic performance testing at model scale (in towing tanks) or even at prototype scale in case of river turbines (Ruopp et al 2014). However, the expensive maintenance costs as well as the problems related to the transport of electricity produced at tens of meters under the sea level are still topical, the exploitation of this type of technology remaining restrained. In case of the power of tidal currents in channels, Garrett and Cummins (2008) show that the power potential is not definitely given by the kinetic energy flux. Indeed, a surprisingly small number of turbines would be necessary to recover the maximum obtainable power, since only part of the cross

section may be used (for navigational and ecological reasons) and if allowance of flow reduction caused by drag on the supporting structures of turbines is made.

Finally, focusing on the Swiss case, the interesting hydrokinetic potential may be identified rather in the energy of free-surface canals than in the one of rivers, in order to limit the environmental impact on the natural water flows. Actually, the exploitation of kinetic energy in the existing infrastructure, as the tailrace and the headrace canals of hydroelectric powerplants or the water treatment stations may add value to this potential and may improve the efficiency of some processes. In addition, one may be added here the potential of residual discharge restitution canals, and why not, of the fish passes.

The present work introduces in a first instance the new (patented) isokinetic turbine concept. Then, the case study is shortly described including the tailrace canal pilot site along with the geometry of the new isokinetic turbine and the investigated operating points. An overview of the numerical simulation modelling is also provided, including: turbulence model, numerical scheme, computational domain, spatial discretization and boundary conditions. The results of the unsteady numerical simulations are first focused on the turbine hydraulic performance characteristic for the two simulated geometries. Finally, the qualitative comparative analysis is focused on the flow configuration into- and around the turbine.

2. NEW ISOKINETIC TURBINE CONCEPT

A new ducted isokinetic turbine for rivers and artificial channels has been designed. The new (patented) concept consists on an axial turbine with two joined concentric runners: an annular turbine runner and a central pump runner (see Figure 1). The aim of the pump runner is to induce a suction effect in the central area in order to increase the axial velocity passing through the turbine runner and consequently the hydraulic efficiency.

To complete, the central bulb houses the generator, the gear box, the main shaft and the bearings. The stator blades, placed at the inlet only of the turbine region, are used to minimize the circumferential velocity component at the outlet of the turbine runner, and implicitly, to reduce the hydraulic losses of the diffuser. An inner diffuser, placed both in the convergent and divergent parts of the duct, is used to separate the fluxes of the turbine and pump regions. In order to cope with the variation of the flow velocity into the canal, the turbine operates at variable speed, while keeping fixed the stator and the runner blades.

Finally, the inlet and the outlet sections of the duct are rectangular, whilst the turbine and the pump regions, including the diffuser flux separator are cylindrical. The turbine is integrated in an exterior rectangular parallelepiped box that facilitates the piling up of several modules on the same cross section of the canal. Moreover, at the inlet, the module is protected by an adapted grating that evacuates the debris, avoiding thus the turbine damage. The assembly of modules is placed on the canal bed using special stakes with a sharp end (facilitates the penetration of the ground) and equipped with a disc with variable height position that allows in the same time a better distribution of the anchoring pressure and the positioning of the turbines at the desired water depth. Such system, coupled with additional anchoring cables comes to secure the assembly position into the river/canal, whatever the structure of the bed ground.

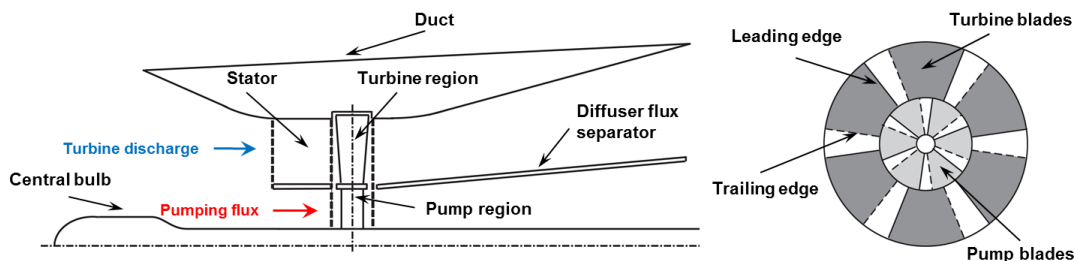


Figure 1. Schematic representation of the new isokinetic turbine concept, patented by Optydro Concept.

The optimization of the hydraulic profile of a turbine with an expected mechanical power of 1 kW is performed using steady incompressible monophasic turbulent flow ($k-\epsilon$ model) numerical simulations. A reduced computational domain including only a periodic quart of the turbine (at prototype scale) immersed in a water box is considered in order to limit the whole CPU time necessary to the whole optimization process. The Fine/Turbo package of the Numeca commercial code is employed to solve the RANS equations using the finite volume method.

The optimal design of the turbine is obtained using a specific procedure described in Kueny et al. (2012). Accordingly, the geometry adapted to the specific initial constraints is generated with the help of HSV specific software (developed by Optydro Concept). Then, the candidate geometries are evaluated with automatic scripts based on the IGG, AutogridV, Fine/Turbo and CFView software of the Numeca CFD suite. Finally, the optimization package is coupled with a software based on an evolutionary strategy completed by an artificial neural network, EASY.

3. CASE STUDY

3.1 Tailrace canal pilot site

The tailrace canal of the Lavey run-of-river powerplant, installed in the Western side of Switzerland on the Rhône River, has been chosen as pilot site in the aim of installing new technologies to recover the energy of rivers and artificial channels. Incompressible unsteady free-surface flow numerical simulations (see Figure 2) have been already performed in the full tailrace canal at prototype scale to investigate its hydrokinetic potential (Hasmatuchi et al. 2014). Moreover, the numerical simulations have been validated with measured axial velocity profiles on 3 different cross sections.

As illustrated in Figure 2, the canal is supplied by the draft tubes of three Kaplan turbines through the tailrace tunnels. Then, the canal presents a strong narrowing at the inlet section downstream the tailrace galleries. The upstream bridge is supported by the two piers that separate the three galleries, whilst the downstream bridge is supported by 2 rectangular piers fixed in the river bed. In red – a fourth gallery planned to be realized in a future development of the powerplant, which is not considered within this work.

Finally, the operating scenario considered in this study consists on constant nominal discharge at the inlet of the three tailrace tunnels. Moreover, the initial flow conditions as well as the inlet velocity profiles at the inlet of the new reduced computational domain are recovered from the converged numerical solution on the full tailrace canal.

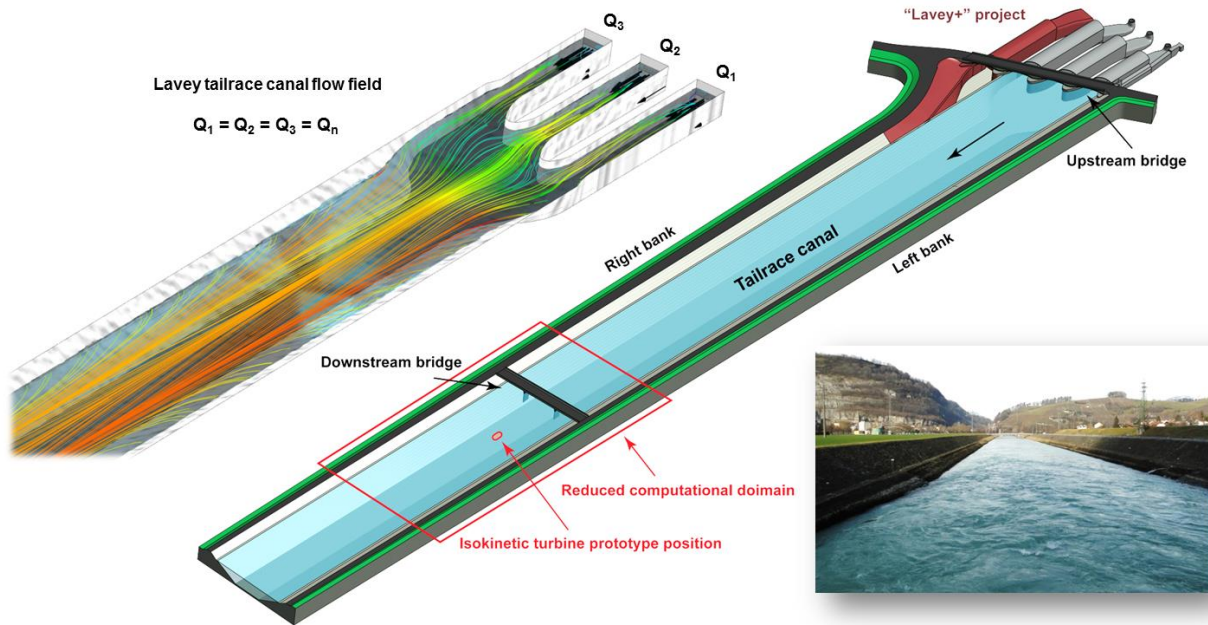


Figure 2. Lavey tailrace canal pilot site, Hasmatuchi et al. 2014.

3.2 New isokinetic turbine prototype

The full geometry of the new isokinetic turbine at prototype scale is illustrated in Figure 3. On the right side, the downstream view of the two different optimized configurations: one with a free central open passage (Case1) and the second one with the central pump runner installed (Case2). The rest of the geometry does not change between the two cases. The duct inlet makes 1 m x 1 m whilst the duct outlet makes 1.5 m x 1.5 m. The total length of the duct is 3 m. The stator exhibits 5 blades, whereas the turbine runner 3 blades and the pump runner 0 or 2, depending on the case. Finally, the turbine runner outer diameter is 1 m and its inner diameter 0.36 m. The pump inner diameter is 0.08 m.

The turbine is placed into the canal at 2.64 m from the bottom in order to benefit of a maximum velocity speed while being sufficiently immersed to avoid free-surface negative impact.

Focusing on the simulated operating conditions, the best efficiency point of each case is first addressed. Then, 4 additional operating points are chosen for each case, respectively: 60%, 80%, 120% and 140% of the nominal runner rotation speed. One may note here that the flow conditions into the canal are kept the same for all investigated operating points.

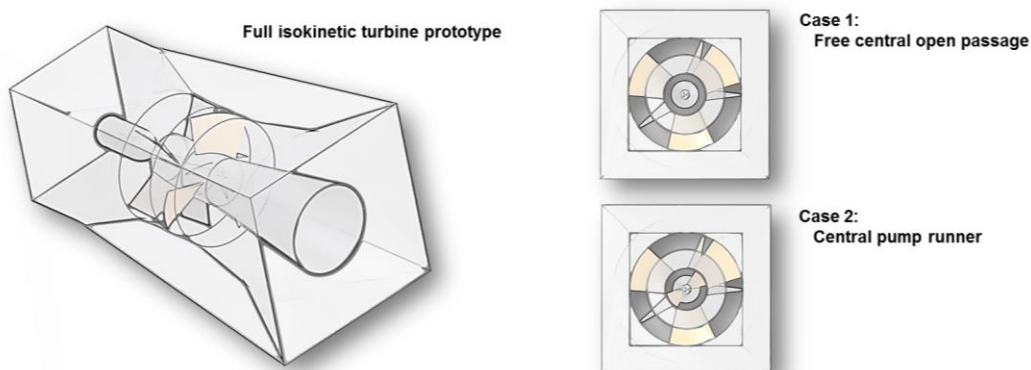


Figure 3. New isokinetic turbine prototype studied configurations: with free central open passage and with central pump runner.

4. MODELLING

4.1 Numerical scheme

Numerical simulations of unsteady incompressible homogeneous multiphase turbulent flow are performed in the full isokinetic turbine immersed into the shorten canal at prototype scale. The numerical setup is summarized in Table 1. The ANSYS CFX 14.5.7 commercial code has been employed to solve both the Unsteady Reynolds-Averaged Navier-Stokes (URANS) equations in their conservative form and the mass conservation equations using the finite volume method (Lauder & Spalding 1974). The set of equations is closed and solved using a two-equation turbulence model and the Shear Stress Transport (SST) model (Menter 1994). Indeed, a blending function that computes the distance from the wall using the solution of a Poisson equation (Menter et al. 2003) is used to select the optimal turbulence model between the $k-\epsilon$ (preferred in the free stream regions) and $k-\omega$ (preferred in the boundary layer) at any location into the domain. An advection scheme (2nd order in space) and the backward Euler implicit scheme (2nd order in time) are used.

The free-surface is captured using the Hirt & Nichols (1981) approach, as in most of the commercial CFD codes based on the volume of fluid method. Moreover, the volume fraction of each fluid in a control volume is calculated in the solution process with the advantage of robustness and capability to deal with highly non-linear free-surface shapes (Godderidge et al. 2008). However, the method is rather computationally expensive. Finally, the multiphase free-surface is solved using the homogenous model. Indeed, the two phases (e.g. air and water) share the same flow field, the transported quantities being the same for both (Harrison et al. 2010). With the volume of fraction specific to the phase, the free-surface is tracked by solving the transport equation for each. The viscosity and the density are volume fraction averaged in the transport equations.

Table 1. Main parameters of the numerical simulation.

Simulation type	Unsteady
Numerical method	Multiphase homogenous
Turbulence model	SST
Time step	4° of runner revolution
Convergence criteria	$RMS_{max} < 10^{-7}$ – 10 internal coefficient t loops
Simulation duration	> 10 runner revolutions

4.2 Computational domain and spatial discretization

As illustrated in Figure 4, the computational domain includes the full shorten tailrace canal water passage at prototype scale, in which the water passage of the new isokinetic turbine prototype is immersed.

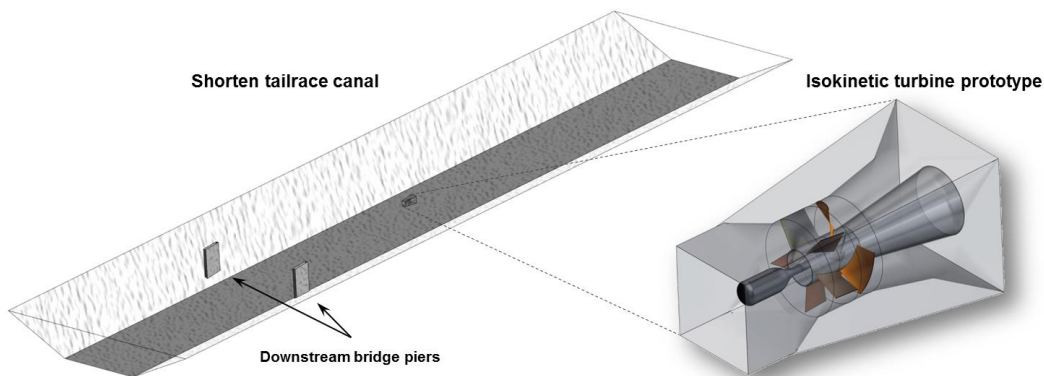


Figure 4. Computational domain including the shorten tailrace canal and the isokinetic turbine at prototype scale.

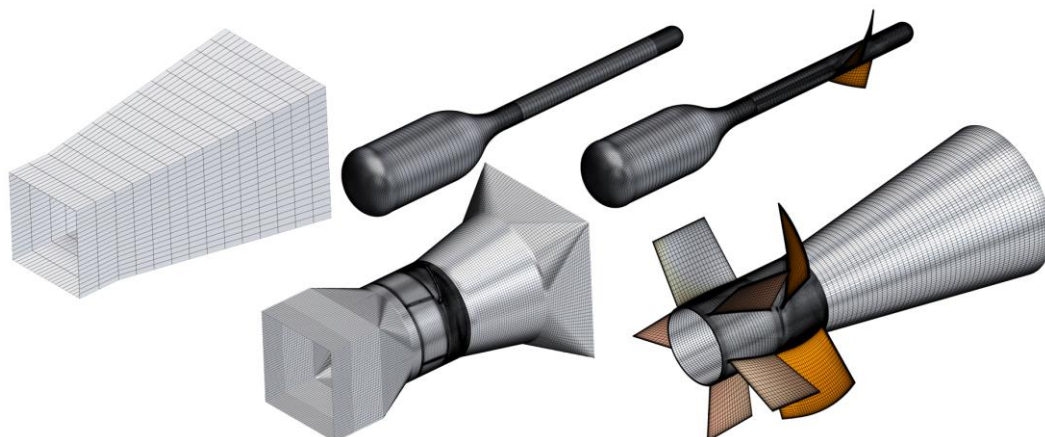


Figure 5. Spatial discretization of the isokinetic turbine prototype.

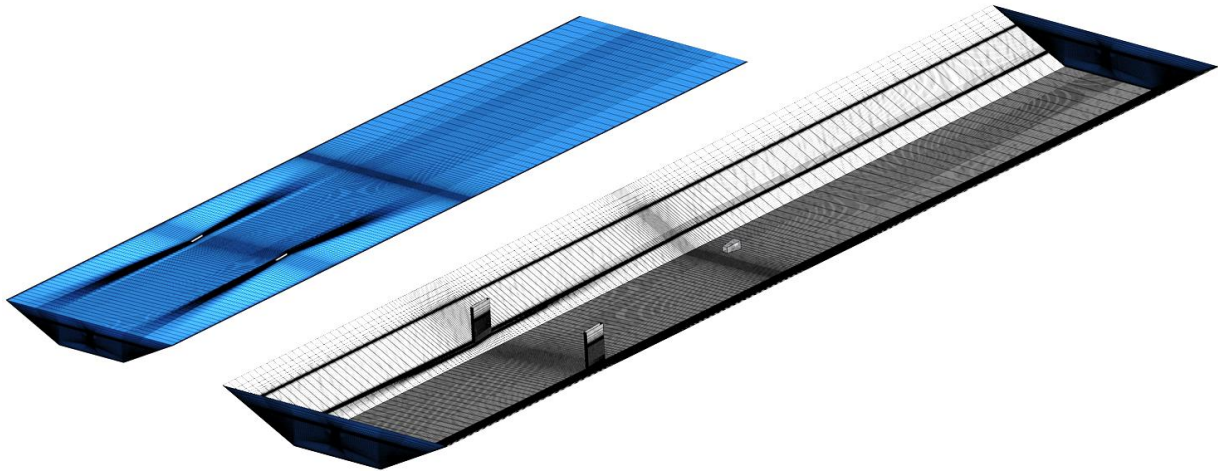


Figure 6. Spatial discretization of the shortened tailrace canal.

An adapted mesh has been generated for both the isokinetic turbine (see Figure 5) and the canal (see Figure 6) with the help of the Ansys Icem commercial software, using mostly structured hexahedral cells. The general mesh size information is provided in Table 2. One may notice here that, on the one hand, an identical mesh is employed for the duct in, stator, turbine runner and duct out domains in both simulated cases. On the other hand, a larger number of nodes are employed for the case with the pump runner installed compared to the case with the free central open passage. Moreover, a slightly larger number of nodes is observed for the shortened canal in the second case, explained by the necessity of a larger refinement region around the free surface. The right refinement around the free surface is actually critical in terms of both residuals convergence and realistic water surface solution.

Table 2. Spatial discretization.

Component	Domain	Case 1		Case 2	
		Number of nodes	y^*_{mean}	Number of nodes	y^*_{mean}
Shorten canal	Stationary	2'284'200	378	2'632'740	350
Duct in	Stationary	850'484	13.24	850'484	13.22
Stator	Stationary	577'800	9.38	577'800	9.31
Turbine runner	Rotating	1'114'830	22.38	1'114'830	22.20
Pump open / runner	Rotating	178'640	12.34	472'150	15.00
Duct out	Stationary	964'830	11.29	964'830	11.67
Full domain		5'970'784		6'612'834	

4.3 Boundary conditions

The detailed boundary conditions imposed on the computational domain including the shortened canal and the turbine are provided in Figure 7. At the inlet of the canal, profiles of velocity components $C_{x,y,z}$, water and air volume fractions $VF_{w,a}$, as well as turbulent kinetic energy k and turbulent dissipation rate ϵ are imposed. The profiles are recovered from a previous converged solution on the full tailrace canal. Then, the water surface level h_{out} along with the hydrostatic pressure profile p_{out} is set at the outlet of the canal. A free slip wall condition is used for the top of the canal and smooth no-slip wall condition on all solid surfaces. Finally, the General Grid Interface (GGI) connection is used to connect the domain of the canal with the one of the turbine, as well as the rotating and stationary domains inside the turbine.

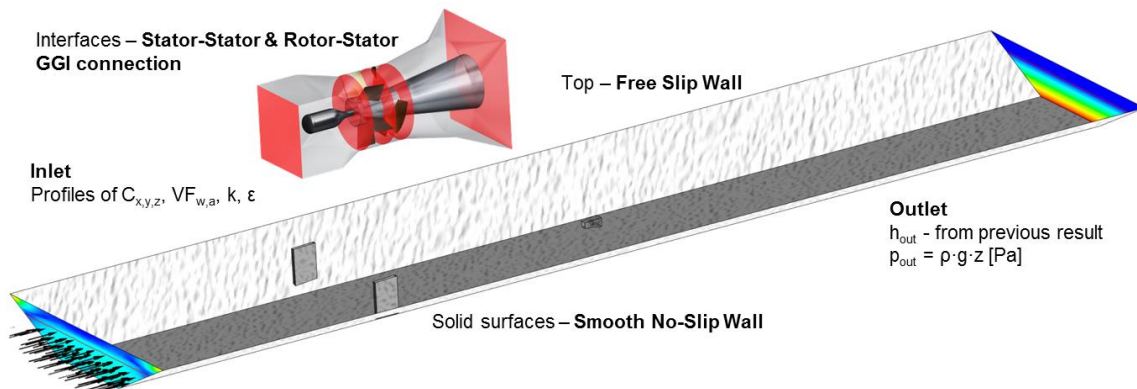


Figure 7. Schematic of boundary conditions.

5. RESULTS AND ANALYSIS

5.1 Convergence

To remember, the numerical simulation convergence criterion has been set to $RMS_{max} < 10^{-7}$. In Figure 8, the RMS of mass and momentum for the two investigated cases at nominal operating condition (dimensionless tip speed ratio $\lambda^* = 1.0$, see Eq. [3]) shows relatively small and stable values over the whole simulation duration. On the same time, the convergence history of the power coefficient (Eq. [1]) shows small fluctuation values only on the last 5 impeller revolutions of simulation, for all operating points. Moreover, the power coefficient fluctuation amplitude is generally smaller for the cases with a free central open passage, compared to the ones with the central pump runner.

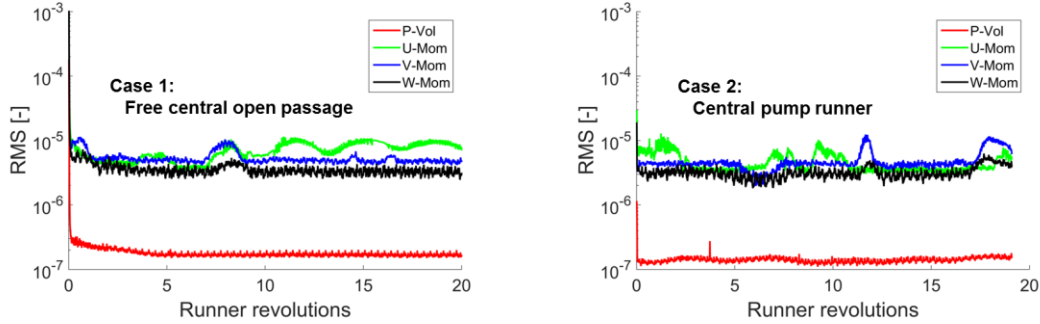


Figure 8. RMS convergence history – case at $\lambda^* = 1.0$ operating conditions.

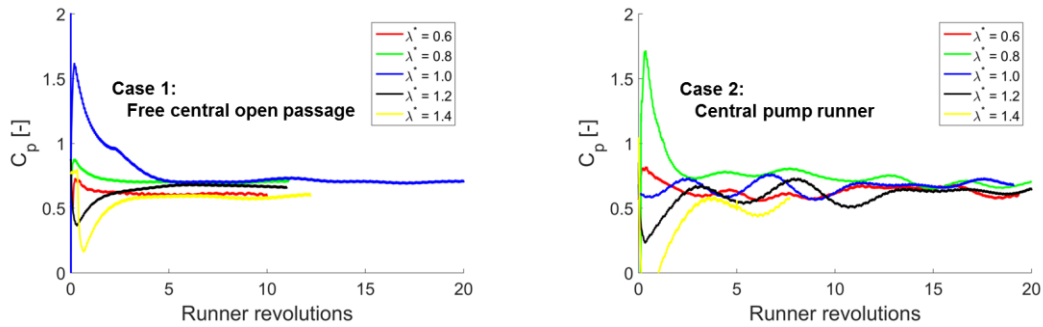


Figure 9. Convergence history of the power coefficient.

5.2 Quantitative analysis

5.2.1 Hydraulic performance

The isokinetic power coefficient is defined in Eq. [1] as the ratio between the mechanical power of the runner and the hydraulic power. The mechanical torque includes values of both the turbine and the pump runners. Moreover, the value of the reference speed C_{ref} is taken at 15 m upstream the duct inlet, which represents a distance equivalent with 5 times the total turbine length. Then, the tip speed ratio λ is defined in Eq. [2], whilst the scaled tip speed ratio λ^* is provided in Eq. [3]. The value of λ_{opt} is taken at the nominal design point for each of the two turbine configurations. Finally, the relation of thrust coefficient is given in Eq. [4].

$$C_p = \frac{\omega \cdot T}{\frac{1}{2} \cdot \rho \cdot \pi \cdot \frac{D_e^2}{4} \cdot C_{ref}^3} [-] \quad [1]$$

$$\lambda = \frac{\omega \cdot \frac{D_e}{2}}{C_{ref}} [-] \quad [2]$$

$$\lambda^* = \frac{\lambda}{\lambda_{opt}} = \frac{\omega}{\omega_{opt}} [-], \text{ for } C_{ref} = \text{ct.} \quad [3]$$

$$C_T = \frac{F_x}{\frac{1}{2} \cdot \rho \cdot C_{ref}^2 \cdot A_{runner}} [-] \quad [4]$$

The hydraulic performance curves for both considered turbine configurations, with central open passage or with central pump runner, can be retrieved in Figure 10. One may state here that the obtained power coefficient is bigger than the Betz limit for a relatively large operating range, whatever the turbine configuration is. This hydraulic performance is explained by the fact that the turbine is ducted. Moreover, the presence of the open passage or of the pump runner induces a suction effect in the central area and implicitly increases the axial velocity passing through the turbine runner. To complete, the hydraulic characteristics of the two configurations are slightly shifted, while reaching almost the same maximum values. The STD values (see the error bars) are in agreement with the convergence history of the power coefficient, plotted in Figure 9. At nominal operating condition ($\lambda^* = 1.0$), the power coefficient is larger for the case with

the central free open passage and relatively the same for the case with the central pump runner, compared to the values obtained during the design and optimization process. This difference may come from the fact that in the present study the numerical simulations are unsteady and include the whole computational domain, whilst during the optimization they were steady and only on a quart of the turbine. Finally, after a new optimization campaign (setting free the parameters of the turbine runner, pump runner and diffuser flux separator, while keeping fixed the rest) a power coefficient bigger than 0.75 is obtained for the case with the central pump runner (see Case 2'). Indeed, the latest proofs the positive effect of the central pump runner presence on the hydraulic performance of the turbine. Anyway, the numerical investigation of this new geometrical configuration makes the object of a future work.

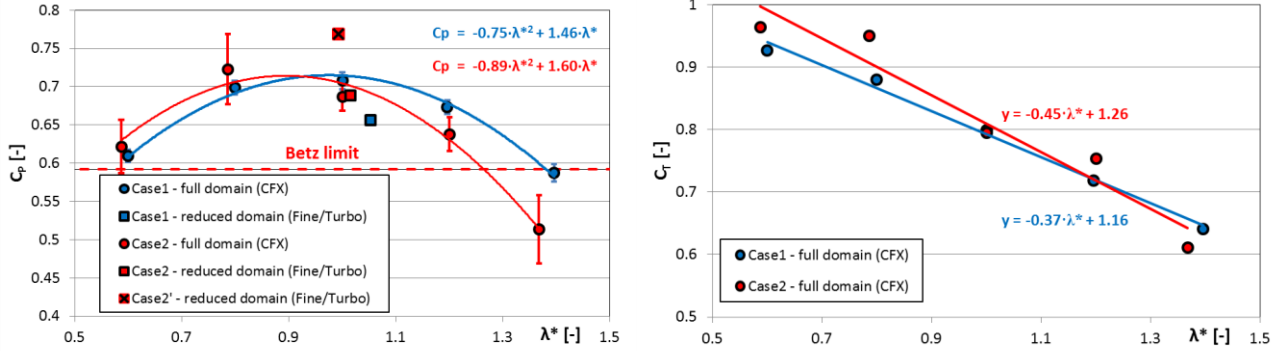


Figure 10. Hydraulic performance curves – time average power coefficient (left) and instantaneous runner thrust coefficient (right).

Focusing on the instantaneous thrust coefficient of the runner (turbine and pump), its value decreases linearly with the scaled speed tip ratio for both cases. The slightly smaller values for the case with the central free open passage, compared to the case with the central pump runner, can be explained by the lower flow resistance in the first case.

5.2.2 Discharge and runner torque distribution

The distribution of the time average dimensionless discharge (Eq. [5]) between the turbine and the pump regions is provided in Figure 11 for both considered configurations. One may state here that the repartition between the turbine and pumping fluxes is almost the same for the two configurations. In addition, a slightly decrease of pumping flux, compared to the turbine one, with the increase of the scaled tip speed ratio can be noticed.

$$Q^* = \frac{Q_{turbine/pump}}{Q_{turbine} + Q_{pump}} \cdot 100 [\%] \quad [5]$$

$$T^* = \frac{T_{turbine/pump}}{T_{turbine} + T_{pump}} \cdot 100 [\%] \quad [6]$$

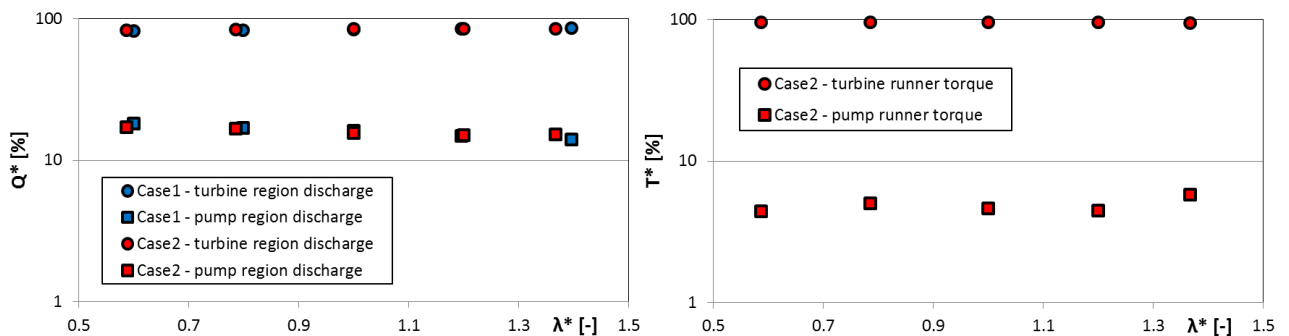


Figure 11. Repartition of discharge (left) and runner torque (right) between turbine and pump regions.

The repartition of the time average dimensionless torque (see Eq. [6]) between the turbine and the pump runners is represented in the right plot of Figure 11 for the case with the central pump runner. On the one hand, the torque of the pump runner is not negative, as expected, but positive, contributing to the total resulting mechanical power. However, the fact that the pump exhibits only 2 blades, compared to the turbine runner made by 3 large blades, allows slightly higher speed values in the central part of the turbine. Indeed, this effect is positive when trying to bypass the Betz effect. On the other hand, more than 90% of the total runner torque is recovered by the turbine blades. Finally, the repartition between the turbine and pump blades seems the same over the whole investigated operating range of the machine.

5.3 Qualitative flow analysis

A first global view of the flow distribution in the whole computational domain is provided in Figure 12 with the help of instantaneous velocity streamlines for the case with the free central open passage at nominal operating point. The represented velocity has been scaled with the average velocity value at 15 m upstream the turbine inlet. One may state

here that the velocity profile on the canal spanwise direction is not perfectly symmetric, but exhibits slightly larger values toward the right bank side. This velocity imbalance (even for the cases when the discharge of the three turbines is equal) is actually explained by the geometrical configuration of the inlet section of the full tailrace canal. Anyway, the flow in the shorten canal is relatively uniform over its full length. The selected implantation position of the isokinetic turbine seems far enough from the downstream bridge piers to avoid an influence of the induced velocity fluctuations at the turbine inlet.

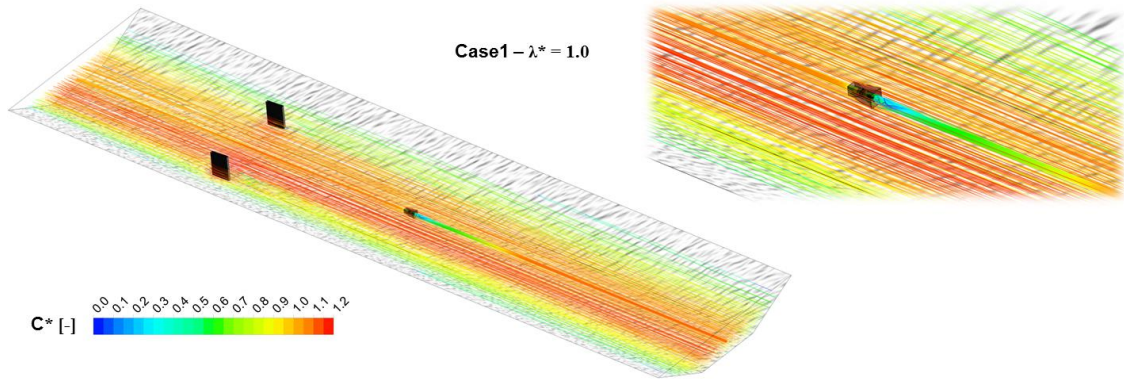


Figure 12. Instantaneous velocity streamlines in the canal.

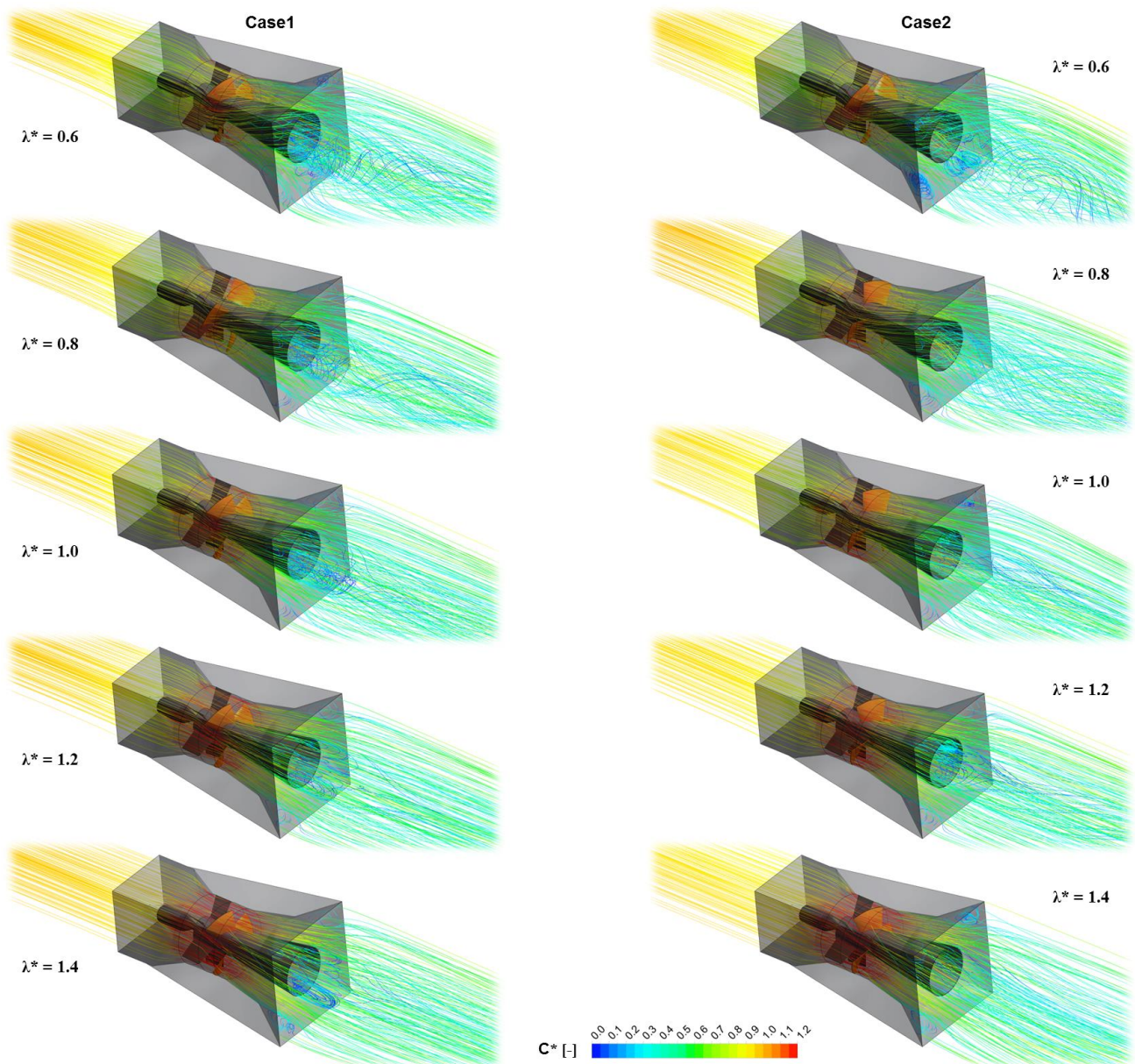


Figure 13. Instantaneous velocity streamlines in the isokinetic turbine.

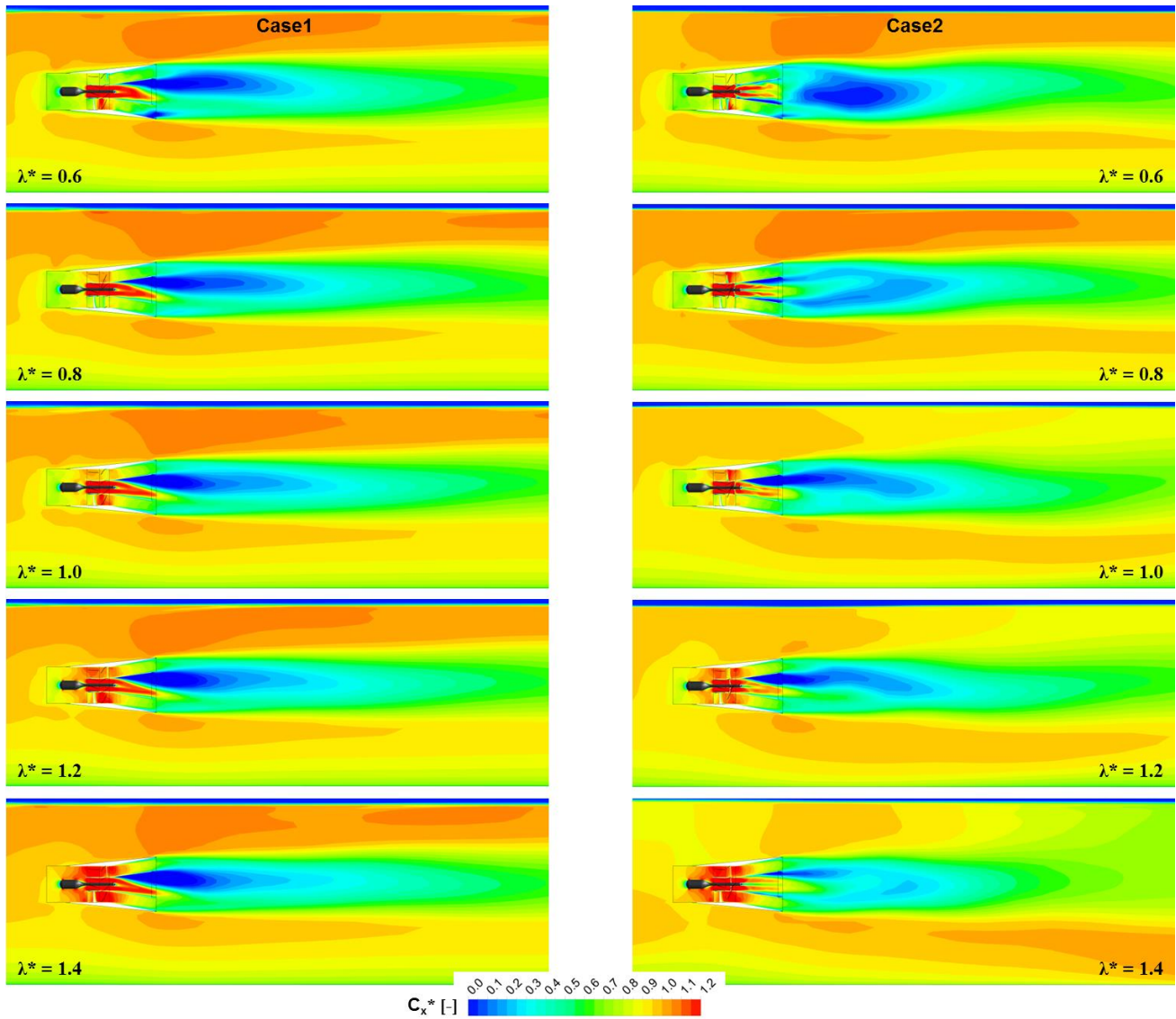


Figure 14. Instantaneous absolute axial velocity contours.

Focusing on the turbine (see Figure 13) the flow at the duct outlet is generally relatively uniform at the periphery, corresponding to the turbine region, whilst it exhibits recirculation in the central part of the duct outlet, corresponding to the pump region. A small flow separation is also noticed at the corners of the duct toward outlet section, due to its rectangular shape. The central stagnation/recirculation region is actually better represented with the help of instantaneous absolute axial velocity contours (see Figure 14) in a longitudinal mid-plane perpendicular to the water surface. Then, the velocity is much larger in the free central open passage and on the pump runner than in the turbine upstream. Indeed, this phenomenon induces a suction effect and allows for larger flowrates in the turbine region as well. In addition, the presence of the pump runner renders the flow axisymmetric in the central part of the turbine (see the Case 2 operating points). This is even further evidenced in Figure 15 by the instantaneous absolute axial velocity contours at the duct outlet. Then, on the interfaces located at the duct inlet, stator inlet and turbine outlet, there is no significant difference between the two cases, excepting the presence of the pump blades wake for the second case. To conclude, the absolute axial velocity generally increases with the increase of the runner rotational speed.

$$c_p^* = \frac{p - \rho \cdot g \cdot z_0}{\frac{1}{2} \cdot \rho \cdot \bar{c}_m^2} \quad [-] \quad [7]$$

Switching the attention to the pressure field, the instantaneous pressure coefficient contours (Eq. [7]) are represented in Figure 17 on the horizontal mid-plane of the turbine. First, the static pressure at the inlet of the duct decreases with the increase of the runner rotation speed for both cases, which is in agreement with the already announced velocity increase. Then, for the case with the central pump runner a central low pressure core is observed in the central diffuser, as an effect of the high swirl velocity at the runner pump outlet.

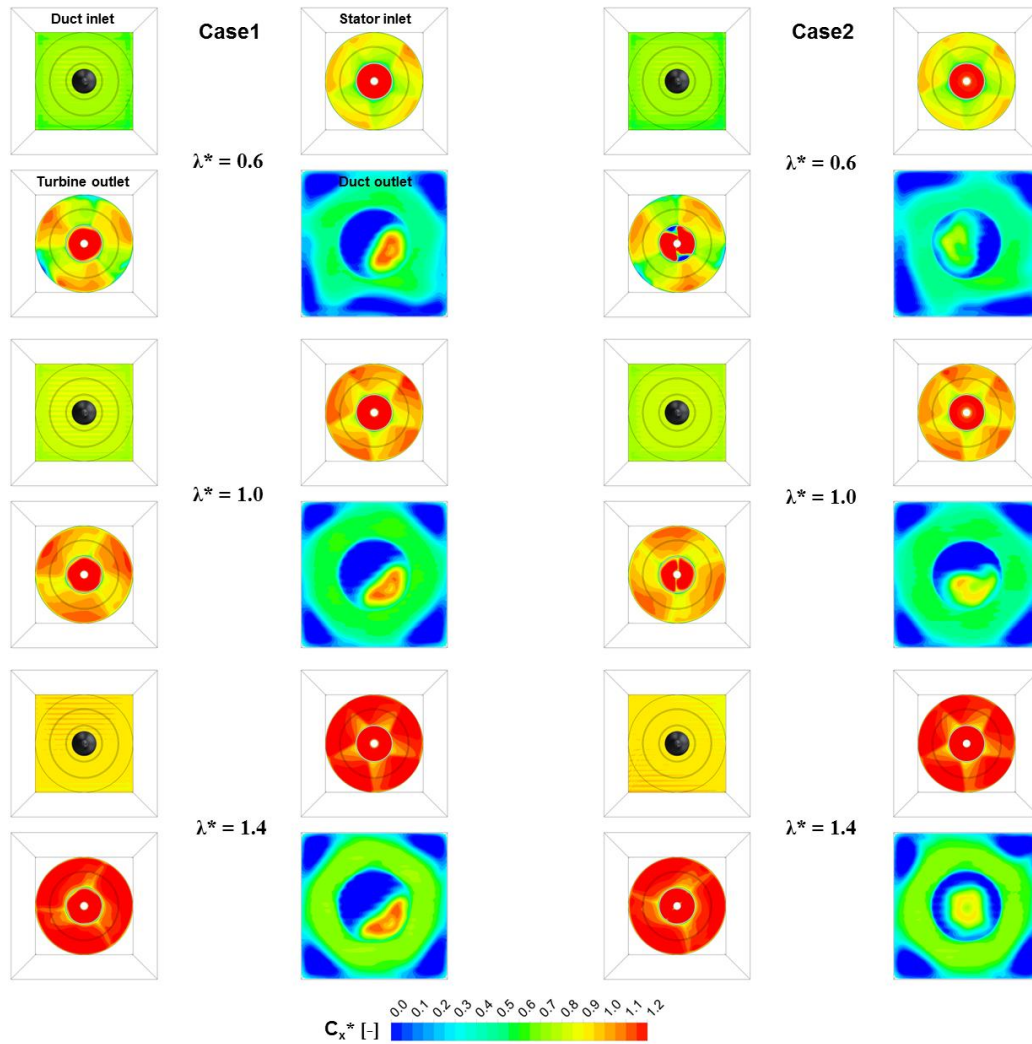


Figure 15. Instantaneous absolute axial velocity contours on different turbine interfaces.

Finally, a comparison on the shape of the water free surface in the canal between the case when the canal is empty and the one with the isokinetic turbine placed downstream the bridge piers is illustrated in Figure 16. One may state here that there is no significant difference between the two cases neither around the location where the isokinetic turbine is placed, nor in the rest of the domain. The small physical and artificial waves on the surface present negligible amplitude. Moreover, they are more or less dependent on mesh refinement around the water surface. Anyway, as presented by Lawn (2003), the ducted turbine may be represented by a resistance coefficient, proportional with the ratio between the pressure drop and the specific kinetic energy of the axial velocity through the runner. For a maximum power, the resistance coefficient must be between 0.5 and 1. Considering the resistance coefficient equal to 1 and the reference velocity from the current case, a maximum theoretical pressure drop is obtained. Indeed, converted in water column, the value does not exceed 0.1 mWC. Actually, this relatively small value explains why no influence is observed on the local water surface level when the machine is placed and runs in the canal. Moreover, the resolution of the mesh grid around the free-surface on the region of the turbine must certainly be higher to capture this relatively small perturbation, compared to the global size of the canal.

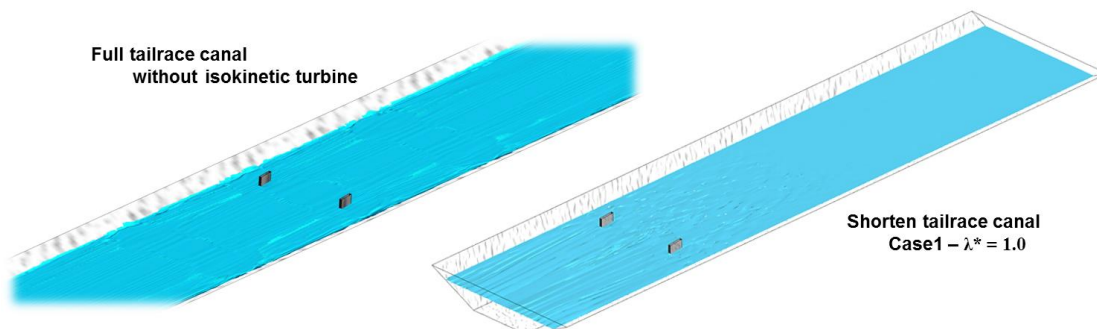


Figure 16. Influence of the isokinetic turbine presence on the canal free-surface.

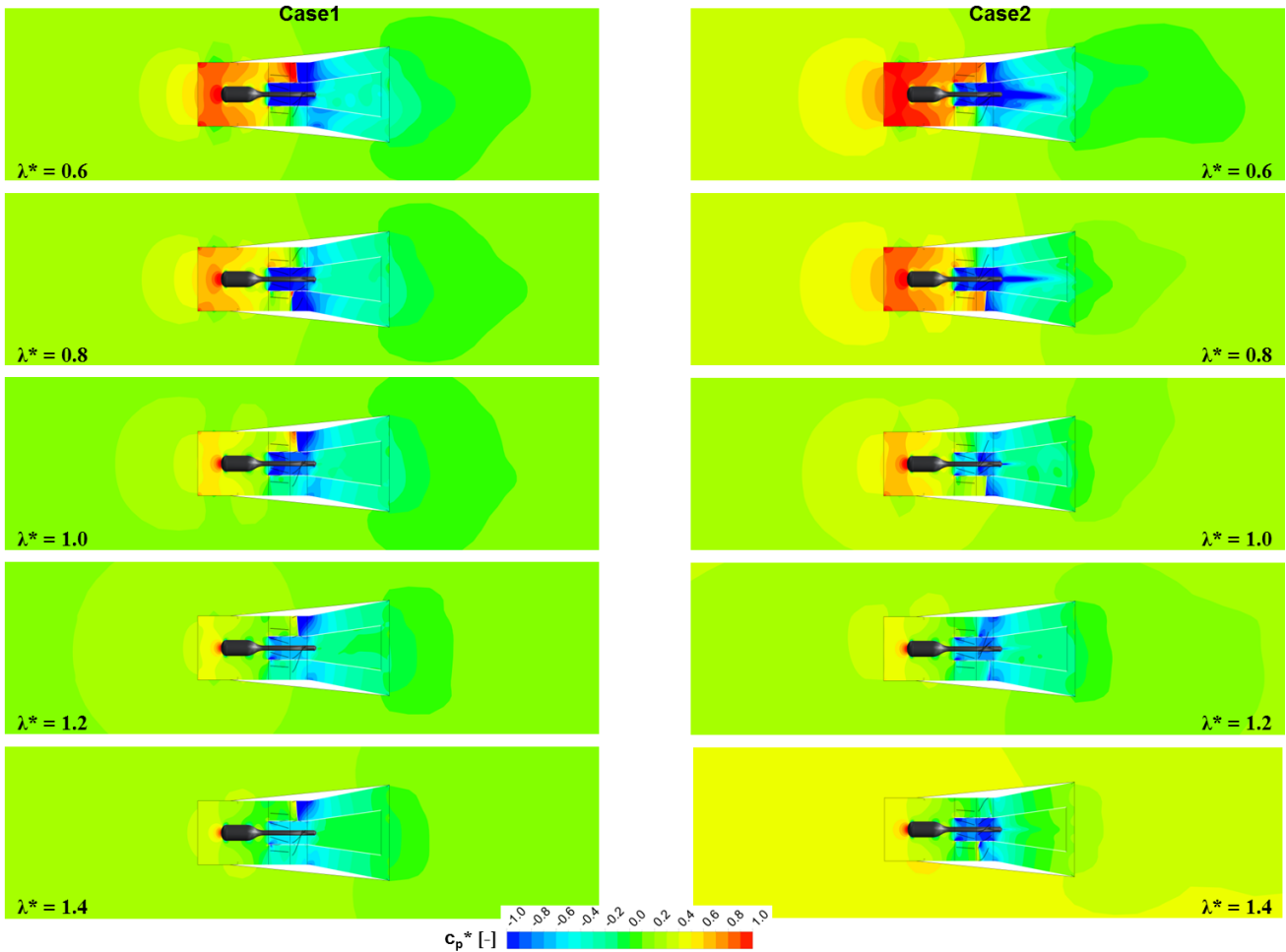


Figure 17. Instantaneous static pressure coefficient contours.

6. CONCLUSIONS

A new 1 kW ducted isokinetic turbine for rivers and canal has been designed. The new (patented) concept consists on an axial turbine with two joined concentric runners: an annular turbine runner and a central pump runner. It has been shown that the pump runner (operating as turbine in the current design) induces a suction effect in the central region, increasing the axial velocity passing through the turbine runner and consequently the hydraulic efficiency. The optimization of the hydraulic profile has been performed using steady incompressible monophasic turbulent flow ($k-\epsilon$ model) numerical simulations. In order to reduce the computational costs, only a periodic quart of the turbine (at prototype scale) immersed in a water box has been considered. The RANS equations were solved with the Numeca Fine/Turbo package using the finite volume method.

Numerical simulations of unsteady incompressible homogeneous multiphase turbulent flow (using the SST model) have been used to recover the hydraulic efficiency of the new isokinetic turbine on a relatively extended operating range of its characteristic. The computational domain includes the full water passage of the final prototype, placed in a in a run-of-river tailrace canal with trapezoidal cross-section. The Ansys CFX 14.5.7 commercial code has been employed to solve the URANS equations, using again the finite volume method.

To conclude, the present work shows a successful implementation of the numerical tools to optimize and to recover the hydraulic efficiency of a new isokinetic turbine with and without the free-surface effects taken into account. In addition, the positive effect of the pump runner presence is assessed by comparing the obtained efficiency with performances of the isokinetic turbine featuring a free central open passage. Finally, the current results may also be used to predict the minimum distance between two consecutive cross-sections necessary in case of installing several machines (or groups) along the canal in order to ensure a maximum recover of energy for all units.

ACKNOWLEDGMENTS

The present numerical investigation was carried out in the framework of Hydro VS applied research project, in partnership with the Laboratory for Hydraulic Machines from École Polytechnique Fédérale de Lausanne, Switzerland, granted by the program The Ark Energy of the Ark – the foundation for innovation in Valais, Switzerland.

The authors would like to address a special thanks to the “Services Industriels de Lausanne” and “Usine de Lavey” industrial partners for their approval and technical support in using the Lavey power plant as case study.

NOMENCLATURE

A	[m ²]	Area	Q^*	[-]	Dimensionless discharge
c_p	[-]	Pressure coefficient	Q_n	[m ³ ·s ⁻¹]	Nominal discharge
\bar{c}_m	[m·s ⁻¹]	Runner outlet average discharge speed	T	[N·m]	Mechanical torque
C_P	[-]	Power coefficient	T^*	[-]	Dimensionless torque
C_{ref}	[m·s ⁻¹]	Reference velocity	$VF_{w,a}$	[-]	Void fraction of water, air
C_T	[-]	Thrust coefficient	y^*	[-]	Dimensionless sublayer-scale distance
C_x	[-]	Dimensionless axial velocity	z	[m]	Vertical Cartesian coordinate
$C_{x,y,z}$	[m·s ⁻¹]	Velocity components	ε	[m ² ·s ⁻³]	Turbulent dissipation rate
D_e	[m]	Runner exterior diameter	λ	[-]	Tip speed ratio
F_x	[N]	Axial force	λ^*	[-]	Scaled tip speed ratio
g	[m·s ⁻²]	Gravity	λ_{opt}	[-]	Nominal tip speed ratio
h	[m]	Water depth	ω	[rad·s ⁻¹]	Runner angular speed
k	[m ² ·s ⁻²]	Turbulent kinetic energy	ω	[s ⁻¹]	Specific dissipation rate
p	[Pa]	Static pressure	ρ	[kg·m ⁻³]	Water density
Q	[m ³ ·s ⁻¹]	Discharge			

REFERENCES

- Belloni C. (2013). Hydrodynamics of ducted and open-centre tidal turbines. PhD Thesis, Balliol College, University of Oxford, Trinity.
- Gaden D.L.F., and Bibeau E.L. (2010). A numerical investigation into the effect of diffusers on the performance of hydro kinetic turbines using a validated momentum source turbine model. *Renewable Energy*, 35, 1152–1158.
- Garrett C., and Cummins P. (2008). Limits to tidal current power. *Renewable Energy*, 33, 2485–2490.
- Godderidge B., Phillips A.B., Lewis S., Turnock S.R., Hudson D.A., and Tan M. (2008). The simulation of free surface flows with Computational Fluid Dynamics. *2008 ANSYS UK User Conference: Inspiring Engineering*, Oxford, UK, October 29 – 30.
- Guney M.S. (2011). Evaluation and measures to increase performance coefficient of hydrokinetic turbines. *Renewable and Sustainable Energy Reviews*, 15(8), 3669–3675.
- Harrison M.E., Batten W.M.J., Myers L.E., and Bahaj A.S. (2010). Comparison between CFD simulations and experiments for predicting the far wake of horizontal axis tidal turbines. *IET Renew. Power Gener.*, 4(6), 613–627.
- Hasmatuchi V., Avellan F., and Münch C. (2014). Numerical modelling of a run-of-river tailrace canal. *Hydro 2014*, Cernobbio, Italy, Paper no. 17.1.
- Heier S. (1998). Grid integration of wind energy conversion systems. Publisher: John Wiley & Sons.
- Hirt C.V., and Nichols B.D. (1981). Volume of Fluid (VOF) method for the dynamics of free boundaries. *Journal of Computational Physics*, 39, 201-225.
- Igra O. (1981). Research and development for shrouded wind turbines. *Energy Conv. & Mgmt.*, 21, 13-48.
- Lago L.I., Ponta F.L., and Chen L. (2010). Advances and trends in hydrokinetic turbine systems. *Energy for Sustainable Development*, 14, 287-296.
- Khan M.J., Bhuyan G., Iqbal M.T., and Quaicoe J.E. (2009). Hydrokinetic energy conversion systems and assessment of horizontal and vertical axis turbines for river and tidal applications: a technology status review. *Applied Energy*, 86(10), 1823–1835.
- Kirke B. (2006). Developments in ducted water current turbines. Sustainable Energy Centre, University of South Australia, source: www.cyberiad.net/library/pdf/bk_tidal_paper25apr06.pdf - accessed on January 2015.
- Kueny J.L., Lalande T., Herou J.J., and Terme L. (2012). Optimal design of a tidal turbine. *IOP Conf. Series: Earth and Environmental Science*, 15(4).
- Lauder B.E., and Spalding D.B.. (1974). The numerical computation of turbulent flow. *Computer Methods in Applied Mechanics and Engineering*, 3(2), 269–289.
- Lawn C.J. (2003). Optimization of the power output from ducted turbines. *Proceedings of the Institution of Mechanical Engineers, Part A: Journal of Power Energy*, 207, 107-117.
- Luquet R., Bellevre D., Fréchou D., Perdon P., and Guinard P. (2013). Design and model testing of an optimized ducted marine current turbine. *International Journal of Marine Energy*, 2, 61-80.
- Menter F.R. (1994). Two-equation eddy-viscosity turbulence models for engineering applications. *AIAA Journal*, 32(8), 1598-1605.
- Menter F.R., Kuntz M., and Langtry R. (2003). Ten years of industrial experience with the SST turbulence model. *Turbulence, Heat and Mass Transfer*, 4, Begell House Inc., 625-632.
- Münch C., Vonlanthen M., Gomes J., Luquet R., Guinard P., and Avellan F. (2009). Design and performance assessment of a tidal ducted turbine. *Proceedings of the 3rd IAHR International Meeting of the Working Group on Cavitation and Dynamic Problems in Hydraulic Machinery and Systems*, Brno, Czech Republic, October 14-16, 571-582.
- O'Doherty T., Mason-Jones A., O'Doherty D.M., Byrne C.B., Owen I., and Wang Y.X. (2009). Experimental and computational analysis of a model horizontal axis tidal turbine. *Proceedings of the 8th European Wave and Tidal Energy Conference*, Uppsala, Sweden, 833-841
- Ruopp A., Ruprecht A., Riedelbauch S., Arnaud G., and Hamad I. (2014). Development of a hydro kinetic river turbine with simulation and operational measurement results in comparison. *IOP Conf. Series: Earth and Environmental Science* 22(6).